Research Signpost
37/661 (2), Fort P.O.
Trivandrum-695 023
Kerala, India

Recent Advances in Pharmaceutical Sciences VI, 2016: 1-16 ISBN: 978-81-308-0566-5
Editors: Diego Muñoz-Torrero, Àngela Domínguez and Àngels Manresa

1. The lipid-protein interplay in efflux pumps

Jordi H. Borrell, M. Teresa Montero, Martha L. Vázquez and Òscar Domènech

Departament de Fisicoquímica, Facultat de Farmàcia and Institut de Nanociència i Nanotecnologia IN2UB, Universitat de Barcelona, 08028-Barcelona, Catalonia, Spain

Abstract. In this work lactose permease (LacY) of *Escherichia coli* has been taken as model efflux pump to investigate the interactions between the protein and the main lipid components (POPE and POPG) of the inner membrane. Two main approaches have been followed: (i) measuring the fluorescence energy transfer between a single tryptophan mutant of the protein (W151/C154G LacY) and pyrene labeled phospholipids (Pyr-PE and Pyr-PG); and (ii) pulling the protein from the supported lipid bilayers where it is embedded by using the tip of the atomic force microscope (AFM). On one hand, fluorescence measurements at different pHs indicate that LacY present selectivity for PE. On the other hand the observations of the reconstituted protein in lipid bilayers by AFM show a preference of LacY for the fluid phase (L_α) rather than for the gel phase (L_β). To get an estimation of the proportion of each lipid in each phase we have constructed a phase diagram for the system POPE:POPG. The diagram shows that at the temperature of the experiments (24 ºC) there is an almost equimolar proportion of each lipid. The results suggest the existence

Correspondence/Reprint request: Dr. Jordi H. Borrell, Departament de Fisicoquímica, Facultat de Farmàcia, UB Av. Joan XXIII, 27-31, 08028-Barcelona, Spain. E-mail: jordiborrell@ub.edu

of a boundary region around LacY formed mainly by POPE laterally segregated from a bulk with a random distribution of POPE and POPG. Force spectroscopy allows to establish the force required and the mechanism to unspecifically unfold the protein.

Introduction

Of major interest in health is the emergence of resistance to antibiotic and anticancer agents. Resistance may originate from several mechanisms: drug inactivation, alteration of the specific target, inactivation of the drug or, active efflux of drug mediated by integral membrane proteins commonly known as multidrug transporters. There are two classes of multidrug transporters: the ABC-type dependent on ATP hydrolysis for pumping out the drugs from the cell; and secondary transporters that extrude drugs via mechanisms that are coupled energetically to the electrochemical potential across the membrane. The extraction of drugs through secondary transporters occurs by pumping the substrate out of the cytoplasm whilst H^+ are uptaken. Transmembrane proteins of this kind are known as antiporters, and most of them belong to the major facilitator superfamily (MFS). Some secondary multidrug transporters of this superfamily include NorA from *Staphyloccocus aureus*, TetA from *Escherichia coli* or LmrP from *Lactococcus lactis*, that confer specific resistance to norfloxacin, tetracycline, and daunomycin respectively [1]. Efflux pump mechanisms are not very well understood but experimental evidence suggests that they depend on the affinity of the drug for the lipid bilayer. Among the mechanistic models proposed for drug resistance the drug always reaches the protein from within the bilayer, suggesting an involvement of the phospholipids in the neighborhood of the multidrug transporters in a coupled mechanism that leads to the expulsion of the drug from the cytoplasm. In this work lactose permease (LacY) of *E. coli*, a paradigm for the secondary transporters belonging to the MFS for which we have convenient engineered mutants, will be used to investigate the interactions with the phospholipids of the bilayer where the protein is embedded. LacY consists of twelve transmembrane α-helices, crossing the membrane in a zig-zag fashion that are connected by eleven relatively hydrophilic, periplasmic and cytoplasmic loops, with both amino and carboxyl termini on the cytoplasmic surface (Fig. 1). By combining molecular biology methods with several biochemical and biophysical techniques LacY was one of the first transmembrane protein for which a tertiary structure was proposed. These studies served as the basis for an

early model of the transport mechanism which was confirmed after obtaining the three-dimensional and two-dimensional crystals. These crystals were obtained from a mutant of LacY, with Gly in place of Cys154 (Cys154 → Gly154; C154G), which is arrested in a stable conformation and yields crystals of sufficient quality for high resolution X-ray diffraction studies [2].

In this work we have investigated the interaction between LacY and the main phospholipids of the inner membrane of *E. coli*. We have delineated two different experimental approaches: (i) Förster resonance energy transfer (FRET) has been applied for the investigation of the boundary region of LacY [3]. The FRET strategy consists on measuring the efficiency of the transference of energy between a single-tryptophan mutant of LacY, used as a donor (D), and phospholipid pyrene derivatives as acceptors (A); and (ii) we have exploited the single molecule force spectroscopy (SMFS) mode of the atomic force microscopy (AFM) [4] to unspecifically pull out LacY from a binary mixture that mimics the inner membrane of *E. coli*.

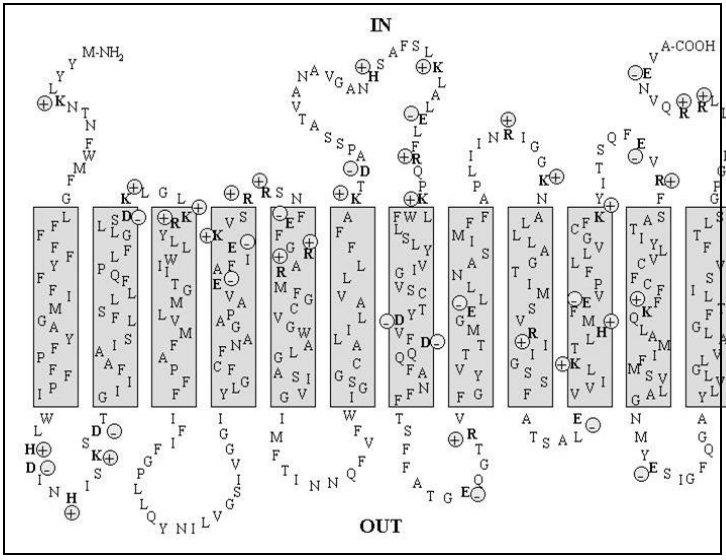

Figure 1. Secondary structure of lactose permease from *Escherichia coli* showing the charged residues (bold). The one-letter amino acid code is used. The putative transmembrane helices are shown in boxes that are connected by hydrophilic loops.

1. Materials and methods

N-Dodecyl-*β*-D-maltoside (DDM) was purchased from Anatrace (Maumee, OH, USA). 1-Palmitoyl-2-oleoyl-*sn*-glycero-3-phospho ethanolamine (POPE), 1-palmitoyl-2-oleoyl-*sn*-glycero-3-[phospho-*rac*-(1-glycerol)] (sodium salt) (POPG), were purchased from Avanti Polar Lipids (Alabaster, AL, USA). 1-Hexadecanoyl-2-(1-pyrenedecanoyl)-*sn*-glycero-3-phosphoglycerol ammonium salt (Pyr-PG) and 1-hexadecanoyl-2-(1-pyrenedecanoyl)-*sn*-glycero-3-phosphoethanolamine ammonium salt (Pyr-PE) were purchased from Invitrogen (Barcelona, Spain). *β*-D-Galactopyranosyl 1-thio-*β*-D-galactopyranoside (TDG), isopropyl-1-thio-ß-D-galactopyranoside (IPTG), and dithiothreitol (DTT) were obtained from Sigma Chemical Co. (St. Louis, MO, USA), and Bio-Beads SM-2 were purchased from Bio-Rad (Hercules, CA, USA). All other common chemicals were ACS grade.

Bacterial strains and protein purification

E. coli BL21(DE3) cells (Novagen, Madison, WI, USA), transformed with plasmid pCS19 encoding single-W151/C154G LacY provided by Dr. H. Ronald Kaback (UCLA, USA), were grown in Luria-Bertani broth at 30 °C containing ampicillin (100 μg/mL) and induced at the appropriate moment with 0.5 mM IPTG. Cells were disrupted and the membrane fraction harvested by ultracentrifugation. Membranes were solubilized by adding DDM and purified by Co (II) affinity chromatography (Talon Superflow^{TM}, Palo Alto, CA, USA). Protein eluted with 150 mM imidazole was subjected to gel filtration chromatography using a Superdex 200 20/30 column (GE-Healthcare, UK), equilibrated with 20 mM Tris-HCl (pH 7.5), 0.008 % DDM. The protein was concentrated by using Vivaspin 20 concentrators (30 kDa cutoff; Vivascience, Germany) and stored on ice. Protein identification was performed by SDS/PGE electrophoresis, and protein quantitation was carried out using a micro-BCA kit (Pierce, Rockford, IL).

Vesicle preparation and protein reconstitution

Chloroform–methanol (2:1, vol/vol) solutions containing appropriate amounts of both labelled and unlabeled phospholipids were dried under a stream of oxygen-free N_2 in a conical tube. The total concentration of phospholipids was calculated as a function of the desired lipid-to-protein ratio (LPR) and protein concentration (1.5 μM). The amount of fluorescent probe was χ =0.015 for all the experiments. The resulting thin film was kept under high vacuum for approximately 3 h to remove organic solvent traces. Multilamellar liposomes (MLVs) were obtained following redispersion of

the film in 20 mM Hepes, 150 mM NaCl buffer, pH 7.40, and applying successive cycles of freezing and thawing below and above the phase transition of the phospholipids, and sonication for 2 min in a bath sonicator. Afterwards, large unilamellar liposomes (LUVs) supplemented with 0.2% of DDM were incubated overnight at room temperature. Liposomes were subsequently mixed with the solubilized protein and incubated at 4 ºC for 30 min with gentle agitation, to obtain a LPR (w/w) of 40. DDM was extracted by addition of polystyrene beads (Bio-Beads SM-2, Bio-Rad).

FRET methodology

Steady state fluorescence measurements were carried out with an SLM-Aminco 8100 (Urbana, IL, USA) spectrofluorometer. The cuvette holder was thermostated with a circulating bath (Haake, Germany), which was used to control temperature within 0.1 ºC. The fluorescence experiments were performed at 25 °C. The excitation and emission bandwidths were 4/4 and 8/8 nm, respectively. For energy transfer measurements single-W151/C154G LacY, the donor, was excited at 295 nm and emission of the pyrene-labeled phospholipids, the acceptor, was monitored at 338 nm. FRET efficiencies (*E*) are calculated according to the equation

$$E = 1 - \frac{I_{\mathrm{DA}}}{I_{\mathrm{D}}} = 1 - \frac{\int_0^\infty i_{DA}(t)dt}{\int_0^\infty i_D(t)dt} \qquad (1)$$

where I_{D} and I_{DA} are the tryptophan emission intensities in the absence or presence of pyrene acceptors, respectively. The reported values of experimental *E* are the averages of triplicate measurements from five separate reconstitutions. In the case of transmembrane proteins, we have to consider the existence of two different populations of phospholipids, those forming the first shell surrounding the protein, confined in the so-called boundary region, and those of the bulk [3]. Assuming these two populations of A molecules, the fluorescence decay of D molecules can be written as

$$i_{DA}(t) = i_D(t)\rho_a(t)\rho_r(t) \qquad (2)$$

where i_D and i_{DA} are the donor fluorescence decays in the absence and presence of acceptor molecules, respectively. Since the number of annular pyrene phospholipids around each protein molecule is expected to follow a binomial population, the annular contribution to the decay can be expressed as

$$\rho_a(t) = \sum_{n=0}^{m} e^{-nk_t t} \binom{m}{n} \mu^n (1-\mu)^{m-n} \tag{3}$$

where m is the number of phospholipid molecules in the first layer surrounding the protein taken as 46 for LacY, μ is defined as the probability of each site in the annular ring being occupied by a labeled pyrene phospholipid and k_t is the rate constant for D-A energy transfer,

$$k_t = \frac{1}{\tau}\left(\frac{R_0}{R}\right)^6 \tag{4}$$

where in turn τ is the donor lifetime and R_0 is the Forster radius (3.0 nm for the Trp/pyrene). On the other hand R, the distance between the D and annular A molecules, can be estimated according to

$$R = \left(w^2 + R_e^2\right)^{1/2} \tag{5}$$

where w is the transverse distance between D and the bilayer centre, and R_e is the exclusion distance along the bilayer plane between the protein axis and the annular lipid molecules. For this system, the value R = 3.2 nm was considered. The geometrical assumptions for FRET measurements are detailed in Fig. 2.

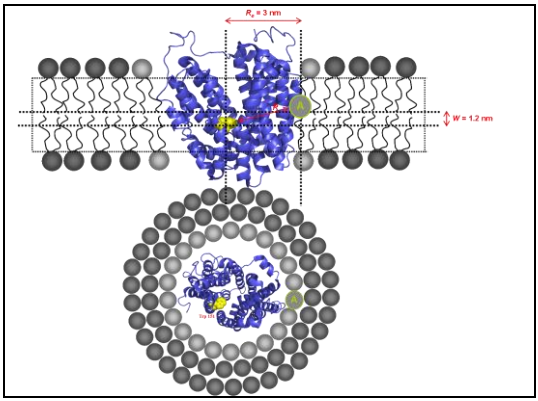

Figure 2. Geometrical assumptions used in FRET modeling. (Up) frontal view showing the location of the donor (Trp151) in yellow and the acceptor (Pyr-PE or Pyr-PG); (Down) sagittal view showing the boundary lipids in light grey where the A are located.

The probability μ can be written as

$$\mu = K_s \frac{n_{pyr}}{n_{pyr} + n_{PL}} = K_s \chi_{pyr} \tag{6}$$

where *n*´s are the mole numbers of the labeled (n_{pyr}) and non-labeled (n_{PL}) phospholipids, χ_{pyr} is the label mole fraction, and K_s is the relative association constant between the labeled and unlabeled phospholipids. Thus, K_s = 1 denotes equal probability of finding acceptors in the annular region and in the bulk, whereas K_s = 0 means no acceptor is in the annular region. Alternatively

$$\mu = \frac{n_{pyr}^{ann}}{n_{pyr}^{ann} + n_{PL}^{ann}} = \chi_{pyr}^{ann} \tag{7}$$

by inserting Eq. 7 into Eq. 6, we obtain a more intuitive meaning of K_s,

$$\chi_{pyr}^{ann} = K_s \chi_{pyr} \tag{8}$$

that is, K_s is the ratio between the acceptor mole fractions in the annular region and in the overall system.

The FRET contribution of acceptors randomly distributed outside the annular region, bulk, can be expressed as

$$\rho_r(t) = \exp\left\{ -4n_2\pi l^2 \int_0^{\frac{1}{\sqrt{l^2+R_e^2}}} \frac{1-\exp\left(-tb^3\alpha^6\right)}{\alpha^3} d\alpha \right\} \tag{9}$$

where n_2 is the acceptor density in each leaflet, l is the distance between the plane of the donors and the plane of acceptors and b being $b = (R_0/l)^2\tau^{-1/3}$.

Supported lipid bilayers and atomic force microscopy

Liposomes or proteoliposomes in Hepes buffer supplemented with 10 mM $CaCl_2$ were deposited onto freshly cleaved mica disks. Samples were incubated at 37 ºC for 2 h in an oven, using a water reservoir to prevent evaporation of the water from the sample. Before imaging, samples were washed with non-calcium-supplemented buffer.

To perform the experiments, it was necessary to drift equilibrate and thermally stabilize the cantilever in the presence of buffer. Images were acquired at 22 ± 0.5 ºC.

Liquid AFM imaging was performed using a Multimode Microscope controlled by Nanoscope V electronics (Bruker, AXS Corporation, Madison, WI). Sample images were acquired in contact mode at scan frequencies of 3 Hz using an optimized feedback parameter and applying minimum vertical force. MSNL-10 V-shaped Si_3N_4 cantilevers (Bruker AFM Probes, Camarillo, CA) with a nominal spring constant of 0.03 $N \cdot m^{-1}$ were used. All images were processed using NanoScope Analysis Software (Bruker AXS Corporation, Santa Barbara, CA).

Force Spectroscopy and protein unfolding

AFM in FS mode was used to obtain nanomechanical magnitudes and to perform protein unfolding [5]. Individual spring constants of the different cantilevers used were determined using the equipartition theorem. Force–distance curves were measured using a constant velocity of 600 $nm \cdot s^{-1}$, with ~1 s of interaction between the AFM tip and the sample surface when protein unfolding was acquired.

The worm-like chain (WLC) model [6,7] was used to fit unfolding events found in the force-distance curves, following the expression

$$F(x) = \frac{k_B T}{4b} \cdot \left((1 - \frac{x}{L})^{-2} - 1 + \frac{4x}{L} \right) \quad (10)$$

where $F(x)$ is the force at a distance x, k_B is the Boltzmann constant, b is the persistence length (0.4 nm) [8], L is the contour length of the unfolded polypeptide chain and T is the temperature. Force peak events of partially unfolded protein were observed in nearly 10% of all force curves, but only experiments with full extension of the protein, that is force curves with force peak patterns with at least 125 nm of extension where used. From these force curves selection only force extensions well-described by the WLC model were accepted for the analysis. All detected unfolding peaks were validated using the root mean square error (RMSE), which is a measure of the difference between the values predicted by the WLC model and the values actually observed. Values with RMSE < 0.015 nN were accepted.

Construction of the phase diagram

A phase diagram for POPE:POPG can be constructed from the excess heat capacity *vs* temperature curves obtained by DSC. Technical details of the experimental procedures have been earlier described [9] .These temperatures are then corrected by the finite width of the transitions of the pure components weighted with their mole fractions. Afterwards, in order to construct a phase diagram of a binary mixture the onset (T_{onset}) and completion (T_{offset}) temperatures observed in the endotherms are plotted against a series of compositions. By connecting the different T_{onset} and T_{offset}, respectively, the solidus and liquidus curves can be defined. A MicroCal MC-2 calorimeter was used for DSC analyses. The data were analysed by the original calorimeter software. The calorimetry accuracy for T_m and for enthalpy changes was ± 0.1 ºC and ± 0.2 kcal mol^{-1}, respectively. Each sample was scanned in triplicate over the temperature range 5-80 °C at a scan rate of 0.44 ºC min^{-1}.

2. Results and discussion

To obtain values of theoretical FRET efficiencies (eq. 1) we have first to solve eq. 3 and 9 and, afterwards inserting the values in eq. 2. As can be seen by inspecting the equations the outcome are μ and K_s. Obviously the accepted outcomes will be those that coincide with the experimental *E*. Details on the development of the model can be found in the literature [10,11] as well as in a review on the applicability to LacY and different levels of lipid-pyrene labeling [3].

Table 1. Experimental efficiencies, probabilities of each site in the boundary region being occupied by a pyrene labelled phospholipid and relative association constant toward LacY.

Labelled lipid (1.5%)	**POPE (98.5%)**			**POPG (98.5%)**		
	E	μ	K_s	*E*	μ	K_s
Pyr-PE	0.79	0.10	6.53	0.66	0.03	2.00
Pyr-PG	0.53	0.00	0.00	0.51	0.00	0.00

In Table 1, the experimental FRET values are listed along with the calculated μ and K_s values. As can be seen μ and K_s could be only calculated for Pyr-PE and never for Pyr-PG. It is worth mentioning that ideally $K_s = 1$ for any probe that mimics the non-labeled phospholipids. Therefore, these $K_s > 1$ may indicate either a boundary region extremely enriched in the label or

that Pyr-PE does not mimic well the unlabeled phospholipid. Since K_s = 0 means no acceptor in the annular region, it becomes clear that Pyr-PG is completely excluded from the boundary. On the other hand, notice that μ and K_s for Pyr-PE in the POPG matrix are compatible with a moderate enrichment of the label in the annular region. All these observations may be likely related with the inverted topology of domains C6 and P7 of LacY (12) when reconstituted in POPG proteoliposomes. Nevertheless, our FRET measurements in POPE and POPG matrices confirm the preference of LacY for PE and its probable predominance in the boundary region.

The requirement of PE for the correct folding and function of LacY has been largely documented [13]. Even a possible specific interaction between PE and some specific amino acid residues of the protein has been postulated [14]. Such interaction could be likely attributed to the ability of PEs to form extensive hydrogen bonds. Hence, variations in the efficiency of FRET should be expected when the pH changes. This phenomena can be observed in Fig. 3, where *E* values at acid, neutral and basic pHs are plotted for POPE:POPG (mol/mol) proteoliposomes doped with Pyr-PE or Pyr-PG (0.1 %).

Actually, whilst POPE is a zwitterion, POPG bears a negative charge at neutral pH. Therefore the decrease of *E* at pH 11 and its increase at pH 3 reported by PyrPE strongly supports the participation of the negative charge of the phosphate group in the interaction with LacY. In agreement, in basic conditions PG would be able to interact and therefore a dramatic increase of

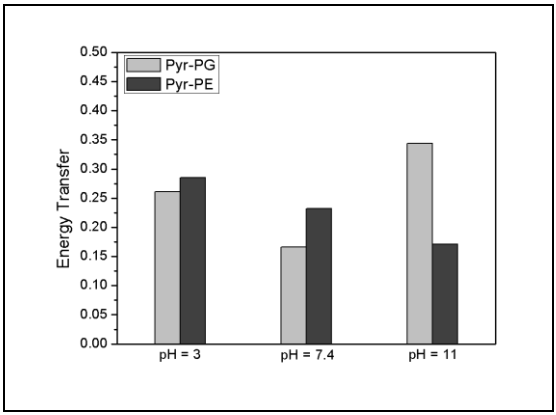

Figure 3. FRET energy transfer at three pH values from single-W151/C154G LacY reconstituted in proteoliposomes of POPE:POPG (3:1, mol/mol) doped with 0.1% of Pyr-PG or Pyr PE.

E values in these conditions is observed. At pH 3, when all groups are protonated, both labels reported a similar FRET efficiency. Interestingly, it has been also reported that PC can support the uphill transport of lactose [15], which emphasizes the fact that the zwitterion character, and the negative charge of the phosphate group are required for LacY proper function.

One interesting property of the POPE:POPG system is that at least in the presence of Ca^{2+} it presents lateral segregation into domains [9]. The presence of divalent cations is required for obtaining the adequate adsorption of the lipids onto the substrate (mica) commonly used to form SLBs. One example of these SLBs is shown in Fig. 4 where the phase separation is clearly observed by the different coloration between the two domains. Noteworthy, in these experiments Ca^{2+} concentration was minimised by swabbing it away after SLB formation. However, the presence of divalent cations between the apical monolayer and the substrate is not excluded.

From the nanomechanical study of these SLBs two magnitudes can be obtained: (i) the yield threshold force (F_y), i.e. the force that the bilayer can withstand before being indented, and (ii) the adhesion force (F_{adh}), i.e. the pull-off force between the tip and the bilayer [16]. Actually, these magnitudes,

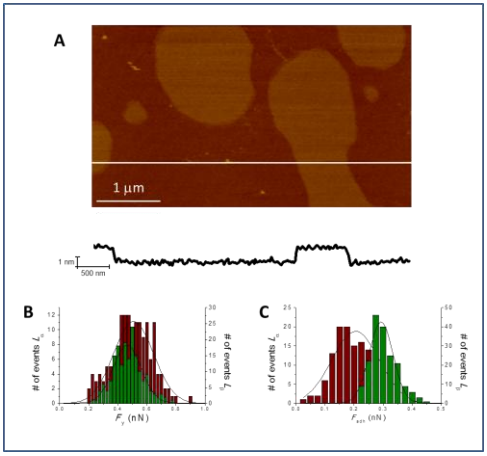

Figure 4. AFM topographic image and height profile analysis of POPE:POPG (3:1, mol/mol) SLB (*Z* scale = 10 nm) (A). Histograms present the distribution of forces of L_α phase (red) and L_β phase (green) for F_y (B) and F_{adh} (C). Fittings to a Gaussian distribution are represented in solid lines. Reprinted from Suárez-Germà *et al.* [5] with permission from Elsevier Science.

particularly F_y, are considered as fingerprints for lipids and phases characterization [16-18]. Distribution of the F_y and F_{adh} values obtained for POPE:POPG are shown in Fig. 4B and 4C, respectively. F_y values ranged from 0.509 ± 0.008 nN to 0.464 ± 0.006 nN and they are characteristic of the gel (L_β) and fluid phase (L_α) of the bilayer, respectively. For F_{adh} we found similar values for both lipid phases, although L_β showed a slightly higher F_{adh} value than L_α (0.292 ± 0.002 nN and 0.205 ± 0.004 nN, respectively).

In order to know the composition of each phase observed, we build a phase diagram of the POPE:POPG system (Fig. 5). A substantial deviation from the ideal mixing behaviour at all the molar fractions is observed. By applying the lever phase rule we can conclude that at 24 ºC, temperature of the AFM observations, we have almost 50% of each phase, which coincides approximately with the distribution of the areas observed in Fig. 4.

Transmembrane proteins tend to insert preferentially into fluid phases. Such is the case of LacY, from which we have already observed this tendency [19]. Thus, when LacY is reconstituted at a LPR (w/w) of 0.5, proteolipid sheets as those shown in Fig. 6A are observed. Similarly, two domains can be distinguished. However, whilst in Fig. 4A, the surfaces were smooth, in Fig. 6A the differences in roughness between both domains is ~ 0.07. The most corrugated domain (higher) contains small entities densely packed that are due to LacY self-segregation into the fluid domains [20].

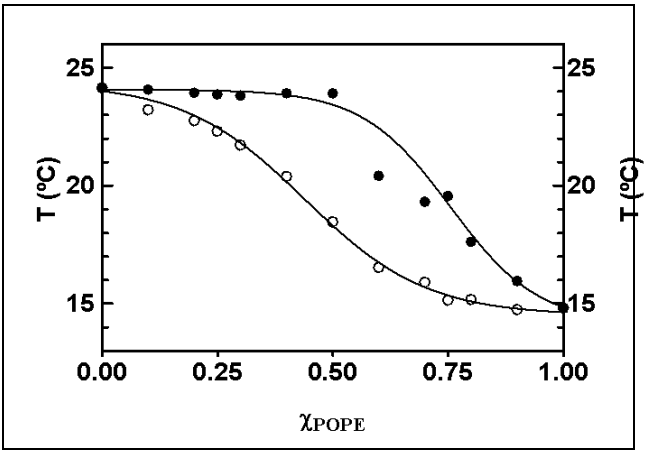

Figure 5. DSC phase diagram for POPE:POPG mixtures obtained from the heat capacity curves (data not shown). Empty circles correspond to the experimental T_{onset} and filled circles to the T_{offset} of the main phase transition.

Interestingly, F_y values for domains with and without LacY were 0.124 ± 0.004 nN and 0.37 ± 0.01 nN, respectively. This indicates a strong perturbation of the system, in both phases, due to the presence of LacY.

The unfolding of LacY from the lipid bilayer where it is embedded by means of force spectroscopy is enhanced in samples where the protein is densely packed as in the high domain in Fig. 6A. The retraction curves of LacY (Fig. 7A), displayed characteristic saw-tooth like pattern of force peaks similar to other secondary transporters characterised by 12 transmembrane α-helix [21,22]. These peaks are characterized by a nonlinear increase in the force as a function of the distance followed by an abrupt drop on force to an ideally zero force value. From the figure we observe some periodicity between the peaks and there are not distinguishable overlapped saw-tooth patterns suggesting that only one protein is pulled out in each event [23]. Indeed, fully extended LacY should present an unfolding curve of about ~170 nm (427 amino acids considering the His-Tag and 0.4 nm per amino acid residue [8]). However the actual representative retracting force-curve in Fig. 7A is shorter. This fact indicates that complete unfolding for a non-specific pulling did not occur most likely due to the strong lipid-protein interactions. For each force-distance curve, several saw-tooth peaks were obtained but only curves displaying at least 6 individual peaks were used. In Fig. 7B, twelve individual superimposed force-distance curves accomplishing

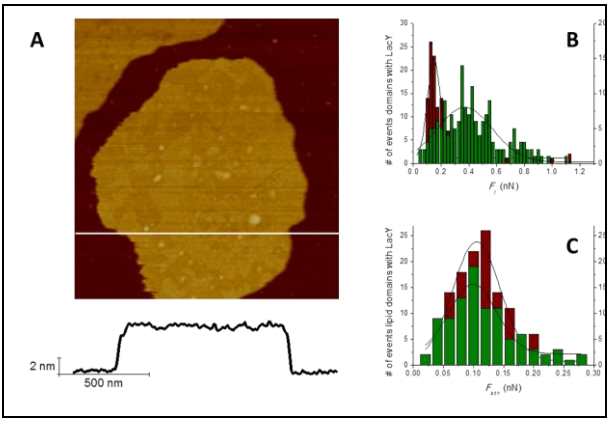

Figure 6. AFM topographic image and height profile analysis of POPE:POPG (3:1, mol/mol) SLB (Z scale = 10 nm) (A). Histograms present the distribution of forces of Lα phase (red) and Lβ phase (green) for F_y (B) and F_{adh} (C). Fittings to a Gaussian distribution are represented in solid lines. Reprinted from Suárez-Germà *et al.* [5] with permission from Elsevier Science.

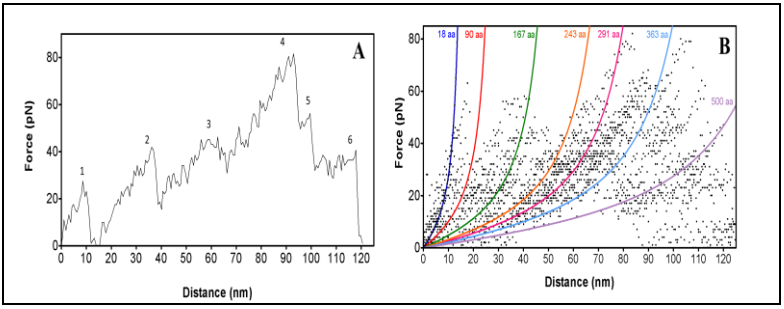

Figure 7. Representative force-distance curve of fully unfolded LacY (A). Superimposed force-distance curves of fully unfolded protein (B). Coloured lines are the WLC curves fitting the mean contour length of individual force peaks while numbering represents the number of amino acids pulled in each event.

the condition demanded are shown. Although there are undefined regions and more data are necessary, the plot becomes significant. There are regions more densely crowded and others with no data at all. To bring some light to the plot we coloured the lines of the WLC curves fitting the mean contour length of individual force peaks. The corresponding number of amino acids pulled out in each event is also shown. We observe that the last curve (purple) represents the extension of 500 amino acids which overcomes the 427 of LacY. This event may result from the complete unfolding of the protein that drags along those phospholipids most likely from the boundary region of LacY.

3. Conclusion

In this work we have observed, by using a bilayer with two phospholipid components that the selectivity of LacY for PE is much higher than for PG. Although PE and PG are both present in almost equimolar proportions in the fluid phase, we do confirm that Pyr-PE is able to get closer to or, alternatively, spend more time next to the LacY. This selectivity is confirmed by FRET measures at different pHs, which suggest the existence of hydrogen bonds between LacY and the phosphatidylethanolamine group. This provides means also for the unfolding patterns obtained when LacY is pulled from the bilayer with the AFM tip. All results indirectly support the hypothesis that bilayer lipids in the neighbourhood of the protein are involved in efflux pump correct folding and function.

Acknowledgements

Thanks to Luis M. Loura and Manuel Prieto for giving us the opportunity to test the FRET model with lactose permease. This work has been supported by the Grant 2014SGR1442 from the Generalitat de Catalunya.

References

1. Van Bambeke, F., Balzi, E., Tulkens, P. M. 2000, *Biochem. Pharmacol*., 60, 457.
2. Abramson, J., Smirnova, I., Kasho, V., Verner, G., Kaback, H. R., Iwata, S. 2003, *Science*, 301, 610.
3. Suárez-Germà, C., Hernández-Borrell, J., Prieto, M., Loura, L. M. S. 2014, *Mol. Membr. Biol*., 31, 120.
4. Müller, D. J., Sapra, K. T., Scheuring, S., Kedrov, A., Frederix, P. L., Fotiadis, D. 2006, *Curr. Opin. Struct. Biol.*, 16, 489.
5. Suárez-Germà, C., Domènech, Ò., Montero, M. T., Hernández-Borrell, J. 2014, *Biochim. Biophys. Acta - Biomembr*., 1838, 842.
6. Bustamante, C., Marko, J., Siggia, E., Smith, S. 1994, *Science* 265, 1599.
7. Janshoff, A., Neitzert, M., Oberdörfer, Y., Fuchs, H. 2000, *Angew. Chem. Int. Ed. Engl*., 39, 3212.
8. Ainavarapu, S. R., Brujic, J., Huang, H. H., Wiita, A. P., Lu, H., Li, L., Walther, K. A., Carrion-Vazquez, M., Li, H., Fernandez, J. M. 2007, *Biophys. J*., 92, 225.
9. Picas, L., Montero, M. T., Morros, A., Cabañas, M. E., Seantier, B., Milhiet, P. E., Hernández-Borrell, J. 2009, *J. Phys. Chem. B*, 113, 4648.
10. Fernandes, F., Loura, L. M., Koehorst, R., Spruijt, R. B., Hemminga, M. A., Fedorov, A., Prieto, M. 2004, *Biophys. J.*, 87, 344.
11. Loura, L.M., Prieto, M., Fernandes, F. 2010, *Eur. Biophys. J*., 39, 565.
12. Dowhan, W., Bogdanov, M. 2009, *Annu. Rev. Biochem.*, 78, 515.
13. Bogdanov, M., Sun, J., Kaback, H. R., Dowhan, W. 1996, *J. Biol. Chem.*, 271, 11615.
14. Hakizimana, P., Masureel, M., Gbaguidi, B., Ruysschaert, J. M., Govaerts, C. 2008, *J. Biol. Chem.*, 283, 9369.
15. Vitrac, H., Bogdanov, M., Dowhan, W. 2013, *Proc. Natl. Acad. Sci.* U. S. A., 110, 9338.
16. Picas, L., Milhiet, P. E., Hernández-Borrell, J. 2012, *Chem. Phys. Lipids*, 165, 845.
17. Garcia-Manyes, S., Sanz, F. 2010, *Biochim. Biophys. Acta - Biomembr*., 1798, 741.
18. Garcia-Manyes, S., Redondo-Morata, L., Oncins, G., Sanz, F. 2010, *J. Am. Chem. Soc.*, 132, 12874.
19. Suárez-Germà, C., Montero, M. T., Ignés-Mullol, J., Hernández-Borrell, J., Domènech, Ò. 2011, *J. Phys. Chem. B*, 115, 12778.

20. Picas, L., Carretero-Genevrier, A., Montero, M. T., Vázquez-Ibar, J. L., Seantier, B., Milhiet, P. E., Hernández-Borrell, J. 2010, *Biochim. Biophys. Acta - Biomembr.*, 1798, 1014.
21. Kedrov, A., Ziegler, C., Janovjak, H., Kühlbrandt, W., Müller, D. J. 2004, *J. Mol. Biol.*, 340, 1143.
22. Kedrov, A., Krieg, M., Ziegler, C., Kuhlbrandt, W., Muller, D. J. 2005, *EMBO Rep*., 6, 668.
23. Oberhauser, A. F., Hansma, P. K., Carrion-Vazquez, M., Fernandez, J. M. 2001, *Proc. Natl. Acad. Sci. U. S. A.*, 98, 468.